Hindawi
Adsorption Science & Technology
Volume 2023, Article ID 5570029, 13 pages
https://doi.org/10.1155/2023/5570029

Research Article

Adsorption of Hydrogen Sulfide on Reduced Graphene Oxide-Wrapped Titanium Dioxide Nanofibers

Kanchit Kamlangkla,[1] Aphichard Phongphala,[1] and Udomdej Pakdee [1,2]

[1]*Division of Physics, Faculty of Science and Technology, Rajamangala University of Technology Krungthep, Bangkok 10120, Thailand*
[2]*Division of Energy Technology for Environment, Faculty of Science and Technology, Rajamangala University of Technology Krungthep, Bangkok 10120, Thailand*

Correspondence should be addressed to Udomdej Pakdee; udomdej.p@mail.rmutk.ac.th

Received 28 May 2023; Revised 30 August 2023; Accepted 20 September 2023; Published 28 September 2023

Academic Editor: Selvaraju Narayanasamy

This work presents a fabrication of room-temperature gas sensor for hydrogen sulfide (H_2S) adsorption. Pristine titanium dioxide (TiO_2) nanofibers, reduced graphene oxide (rGO) sheets, and reduced graphene oxide-wrapped titanium dioxide (rGO-wrapped TiO_2) nanofibers were presented in the form of integrated suspension used for a gas-sensing layer. The TiO_2 nanofibers were firstly synthesized by using an electrospinning method with a polyvinylpyrrolidone (PVP) polymer. The rGO sheets were then wrapped around TiO_2 nanofibers by a hydrothermal method. Scanning electron microscope, transmission electron microscope, X-ray diffractometer, and Raman spectrometer confirmed the presence of rGO sheets onto the surface of TiO_2 nanofibers. Ultraviolet-visible spectrophotometer was also considered and displayed to calculate the band gap of TiO_2 and rGO-wrapped TiO_2 nanofibers. After preparing the gas-sensing suspensions, they were dropped onto the polyethylene terephthalate substrates with silver-interdigitated electrodes. The gas-sensing properties of sensors were evaluated for H_2S adsorption at room temperature. Based on the results, the rGO-wrapped TiO_2 nanofiber gas sensor exhibited higher H_2S sensitivity and selectivity than pristine TiO_2 nanofiber and pure rGO gas sensors. The H_2S-sensing mechanism of rGO-wrapped TiO_2 nanofiber gas sensor was discussed based on a formation of p-n heterojunctions between p-type rGO sheets and n-type TiO_2 nanofibers. Furthermore, a direct charge-transfer process by physisorption was also highlighted as a second H_2S-sensing mechanism.

1. Introduction

Hydrogen sulfide (H_2S) is an extremely harmful and flammable gas. It smells like rotten eggs at low concentration in the air. The harm of H_2S is dependent on its concentration and exposure time. A short-term exposure to over 500-1000 ppm of H_2S is immediately fatal [1]. Repeated exposure to H_2S in concentrations even 10-500 ppm can cause serious damage to organs and central nervous system [1–3]. Therefore, the sensor for the detection of H_2S is required to be developed with high sensitivity and fast response at low concentration. In the past several decades, the metal oxide semiconductor (MOS) nanostructures have become one of the popular materials in gas-sensing applications. The MOS gas sensors have been led to the adsorption in toxic gases [4–6]. However, the adsorption of most H_2S needs to operate at high temperatures [7, 8], although some types of MOS gas sensors can be operated at room temperature under the influences of humidity [9–13]. The MOS provides a large number of free electrons in the conduction band and oxygen vacancies on the surface of the metal semiconductors, resulting in strong adsorption characteristics and high reactivity on the surface of gas molecules [14–17]. Among various MOS materials, titanium dioxide (TiO_2) and its composite have been reported as a popular material for applications in lithium-ion storage [18, 19] and photoelectrocatalysis [20–22]. Due to its strong oxidizing power, abundant existence in nature, nontoxicity, and long-term

physical and chemical stabilities, TiO_2-based gas sensor has been widely used as an efficient gas absorber [23–29]. However, its application has been restricted because of issues such as a low sensitivity, poor selectivity, large band gap, and high operation temperature. Recently, graphene, graphene oxide (GO), and reduced graphene oxide (rGO) have been accepted as a good candidate for improving the functional properties of metal oxide at room temperature [30–36]. It has been very sensitive to chemicals owing to its monolayer structure such as high thermal conductivity, high specific surface area, and high electron mobility at room temperature. However, it has still low sensitivity, poor selectivity, and slow recovery capability which is not suitable for gas-sensing applications. The hybrid nanostructures based on p-type rGO and n-type TiO_2 semiconductors have been mentioned to the formation of p-n heterojunctions, resulting in the enhancement of gas-sensing properties for the nanocomposite materials [37, 38]. The hybrid nanostructures of graphene and semiconductor metal oxide have mainly prepared by electrospinning and hydrothermal processes [38–40]. The electrospun nanofibers have been reported in the special properties such as high specific surface area and porosity [40–43]. Therefore, they are beneficial for application in gas sensor or gas absorber. More importantly, there have not been many publications for the use of rGO-wrapped TiO_2 nanofibers as a room-temperature H_2S gas sensor although some works on fabrication methods of TiO_2 nanofibers followed by TiO_2 wrapped with rGO have been reported [19, 44].

In this work, we have synthesized rGO-wrapped TiO_2 nanofibers by using a combination of electrospinning and hydrothermal methods. The samples were characterized by a scanning electron microscope (SEM), a transmission electron microscope (TEM), an X-ray diffractometer (XRD), a Raman spectrometer, and an ultraviolet-visible (UV-Vis) spectrophotometer. The sensing performance of rGO-wrapped TiO_2 nanofiber gas sensors was systematically evaluated, relating to the sensitivity, selectivity, and stability properties for H_2S adsorption at room temperature. The pristine TiO_2 and pure rGO gas sensors were also fabricated and evaluated as comparisons. The H_2S-sensing mechanism of rGO-wrapped TiO_2 nanofibers is discussed based on the formation of p-n heterojunctions. Furthermore, a direct charge-transfer process by physisorption is also highlighted as a second possible H_2S-sensing mechanism.

2. Materials and Methods

2.1. Preparation of rGO-Wrapped TiO_2 Nanofibers. The preparation process of TiO_2 solution is shown in Figure 1(a). Firstly, 0.9 g polyvinylpyrrolidone (PVP) polymer was dissolved and stirred in 10 ml ethanol for 1 h. During stirring, 2 ml tetrabutyl titanate (TBT) and 1 ml acetic acid (CH_3COOH) were added into the solution. The mixed solution was continuously stirred for 1 h to obtain a homogeneous precursor solution. To prepare the electrospinning TiO_2 nanofibers, the TiO_2 solution was then loaded into a plastic syringe with a small metallic nozzle. It was fixed on a syringe pump and connected to a high voltage power supply of 18 kV. The distance between the nozzle and an aluminium rolling collector was 15 cm. The collector was controlled by a DC motor controller with a fixed angular speed of 0.5 rpm. A sheet of TiO_2 nanofibers was continuously accumulated on a rolling collector for 40 min. The schematic illustration for preparing the TiO_2 nanofiber by using electrospinning method is shown in Figure 1(b). Inset shows a photograph of nanofiber sheet on a rolling collector. After the electrospinning process, the as-spun TiO_2 nanofibers were heated at a fixed temperature of 500°C for 2 h to decompose PVP and crystallize TiO_2.

For preparation of rGO-wrapped TiO_2 nanofibers, a sheet of accumulated TiO_2 nanofibers was crushed with a clean mortar and pestle. Then, 50 mg of GO was dissolved in a solution containing 20 ml of dimethyl sulfoxide (DMSO) and 20 ml of deionized (DI) water under ultrasonication for 2 h. At a same time, 70 mg of TiO_2 nanofibers was then added into the solution to obtain a homogeneous suspension. Then, it was transferred to a 40 ml Teflon autoclave and heated up to 180°C for 10 h. After that, it was then rinsed several times with DI water and dried at 70°C for 12 h. Finally, the rGO-wrapped TiO_2 nanofibers were obtained. For preparation of rGO sheets, the GO powder was treated at the same condition without TiO_2 nanofibers. The schematic illustration of rGO-wrapped TiO_2 nanofibers in preparation process is shown in Figure 1(c). The samples were examined by SEM (Quanta 450 FEI), TEM (Hitachi HT7700), XRD (Bruker D8 Advance), and Raman spectrometer (Perkin Elmer Spectrum GX). The UV-Vis spectrophotometer (Perkin Elmer Lambda 950) was conducted and displayed to calculate the band gap of samples.

2.2. Fabrication of rGO-Wrapped TiO_2 Nanofiber Gas Sensor. To prepare the rGO-wrapped TiO_2 nanofiber gas sensor, the dried powder of rGO-wrapped TiO_2 nanofiber (20 mg) was dispersed in 1 ml DI water and 1 ml ethanol under ultrasonication for 5 min. Then, the suspension was dropped onto a polyethylene terephthalate (PET) substrate with silver-interdigitated electrode (Ag-IDE) and dried at room temperature. Figure 2 shows the photograph of dimensional Ag-IDE before and after drop-casting with 20 μl rGO-wrapped TiO_2 nanofiber-sensing suspension. It is seen in Figure 2(a) that the width and the interdigit spacing of the electrode are found to be ~1.0 mm. The size of a drop-casted sensing suspension is approximately 5.0×10.0 mm^2, as shown in Figure 2(b).

2.3. Gas-Sensing Measurement. The gas-sensing properties of pristine TiO_2 nanofiber, rGO, and rGO-wrapped TiO_2 nanofiber gas sensors were evaluated on their performances by using a gas-measurement system. The system consists of a tank of H_2S, a tank of pure air, two mass flow controllers, a mixer, a test chamber, a circuit board, a power supply, a digital multimeter, and a ventilator. The fabricated gas sensor was loaded into a test chamber which is connected to a voltage divider circuit. The H_2S and pure air were used as target and background gases, respectively. The sensing signals were determined by the measurement of sensor resistance in every second when they were exposed to target and

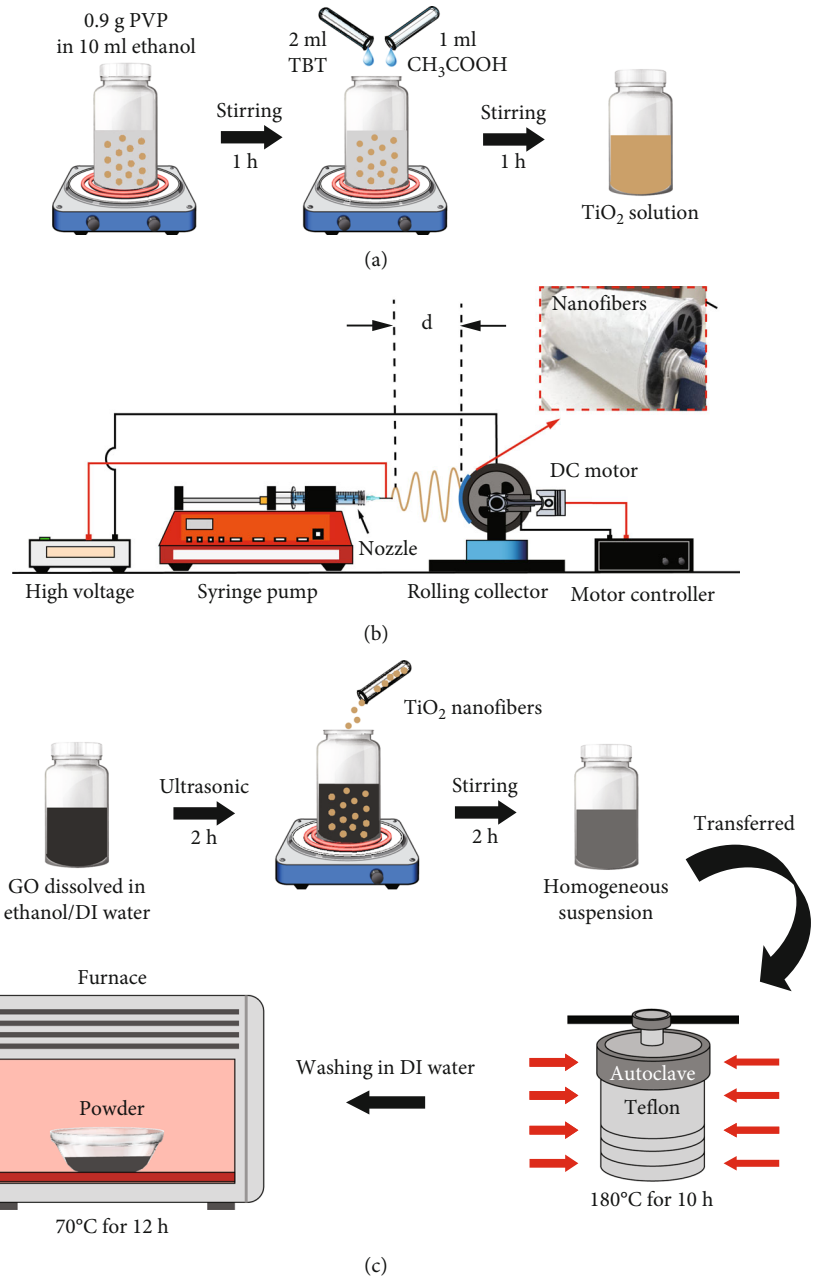

Figure 1: Schematic illustration of preparation for (a) TiO_2-based solution, (b) electrospun-TiO_2 nanofibers (inset shows a photograph of nanofiber sheet on a rolling collector), and (c) rGO-wrapped TiO_2 nanofibers.

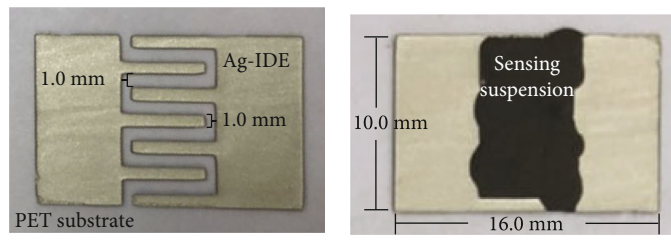

Figure 2: Photograph of dimensional Ag-IDE (a) before and (b) after drop-casting with a sensing suspension on PET substrate.

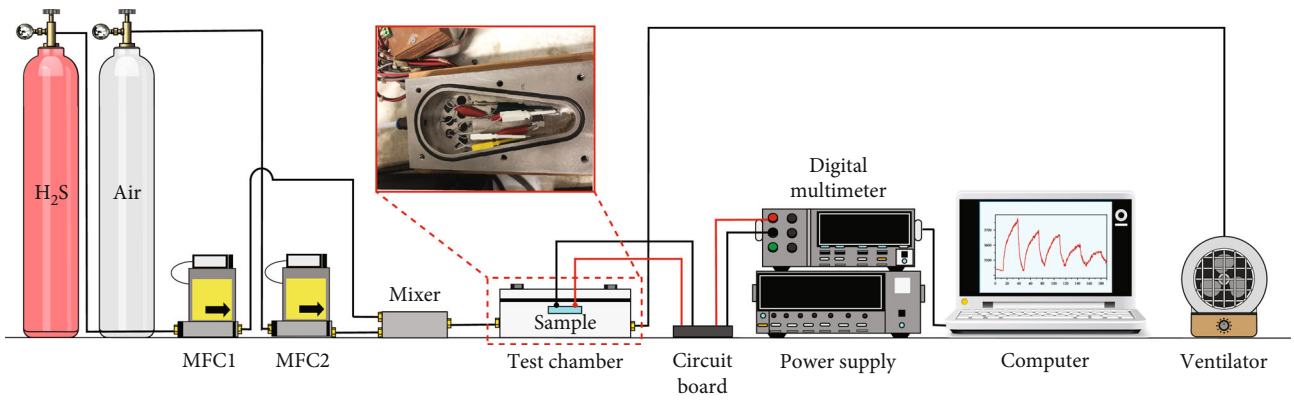

FIGURE 3: Schematic illustration of gas-measurement system (inset shows a photograph of stainless-steel chamber with electrical signal wires).

background gases. The signals were monitored by a laptop computer operated with a program in LabVIEW software. After the measurement, the remaining gas was removed out of the chamber by the ventilator. The schematic illustration of gas-measurement system is displayed in Figure 3.

3. Results and Discussion

3.1. Morphological, Structural, and Electronic Properties of rGO-Wrapped TiO_2 Nanofibers. The morphologies of a graphene oxide (GO) sheet, TiO_2 nanofibers, and rGO-wrapped TiO_2 nanofibers are displayed by TEM and SEM images, as shown in Figure 4. Figure 4(a) demonstrates TEM image of a GO sheet in DMSO solvent. It is seen that the GO sheets in DMSO solvent are well spreadable. Therefore, the DMSO solvent is a good candidate for GO spread and dispersion without having an effect on the quality of GO structure. Moreover, the surfaces of TiO_2 nanofibers examined by SEM (Figures 4(b) and 4(c)) seem to be smooth due to the low viscosity of the solutions during the electrospinning process. After the hydrothermal process, the rGO sheets were wrapped around the surface of TiO_2 nanofibers with nonuniform distribution due to the continuous sonication. The morphology of rGO-wrapped TiO_2 nanofibers is displayed by TEM image, as shown in Figure 4(d). Moreover, the rough surface of rGO-wrapped TiO_2 nanofibers can be observed in Figures 4(e) and 4(f). It may be due to the deformation of PVP polymer after the heat-treatment process. The diameter distributions of TiO_2 and rGO-wrapped TiO_2 nanofibers were analyzed from different areas of various SEM images by using ImageJ software. As shown by histogram graphs in inset of Figures 4(b) and 4(e), the diameter distributions of TiO_2 and rGO-wrapped TiO_2 nanofibers can be found in the range of 57 ± 19 nm and 81 ± 15 nm, respectively.

Figure 5 shows TEM image of rGO-wrapped TiO_2 nanofiber and its elemental map. It provides information to support the above statement about the existence of titanium (Ti), oxygen (O), and carbon (C) elements on the surface of sample. The energy-dispersive X-ray spectroscopy (EDS) mapping affirms uniform distribution of Ti, O, and C elements for the rGO-wrapped TiO_2 nanofibers, as shown in Figure 5. The atomic percentages of rGO/TiO_2 nanocomposite are 58.83% (Ti), 29.94% (O), and 11.23% (C).

Figure 6 shows the XRD patterns of pristine TiO_2 nanofibers and rGO-wrapped TiO_2 nanofibers. The 2θ peaks of 25.2° (101), 37.8° (004), 48.1° (200), 55.2° (221), and 62.7° (118), according to JCPDS file number 21-1272, corresponding to the anatase TiO_2 are observed (see Figure 6(a)). This pattern presents a reference in the comparison between pristine TiO_2 and rGO-wrapped TiO_2 nanofibers. As can be seen in Figure 6(b), the more 2θ peaks of 27° (110), 41° (111), 44° (210), and 69° (301), according to JCPDS file number 88-1175, corresponding to the rutile TiO_2 can be also observed. The percentages of rutile (W_R) and anatase (W_A) phases for the TiO_2 can be calculated from the intensities of the rutile (I_R) and anatase (I_A) peaks in XRD [45], as defined by

$$W_R(\%) = \frac{1}{1 + (I_R/0.8I_A)} \times 100, \quad (1)$$

$$W_A(\%) = 100 - W_R. \quad (2)$$

It is observed that the rutile percentage of pristine TiO_2 nanofibers is 0%, while the anatase percentage is 100%. For the rGO-wrapped TiO_2 nanofiber sample, it contains 29.03% rutile and 70.97% anatase. Therefore, the calculated ratio between anatase and rutile phases of the rGO-wrapped TiO_2 nanofibers is found to be 2.4. Furthermore, the XRD pattern of TiO_2 nanofibers reveals only peaks for the anatase phase, while the XRD pattern of rGO-wrapped TiO_2 nanofibers reveals different peaks for rGO, anatase, and rutile phases of TiO_2. However, the diffraction peaks of rGO at 24.5° cannot be observed separately.

The existence of rGO sheets on TiO_2 nanofibers was confirmed by Raman spectra, as displayed in Figure 7. It is seen in Figure 7(a) that the Raman spectrum of rGO-wrapped TiO_2 nanofibers presents the four peaks of $E_g(1)$, $B_{1g}(1)$, $A_{1g}(1)$, and $E_g(2)$ around 140 to 640 cm^{-1} attributed to the vibration modes of anatase and rutile TiO_2 [46, 47]. For the pristine TiO_2 nanofibers, the peak of Raman spectrum from the rutile TiO_2 is not observed. However, the

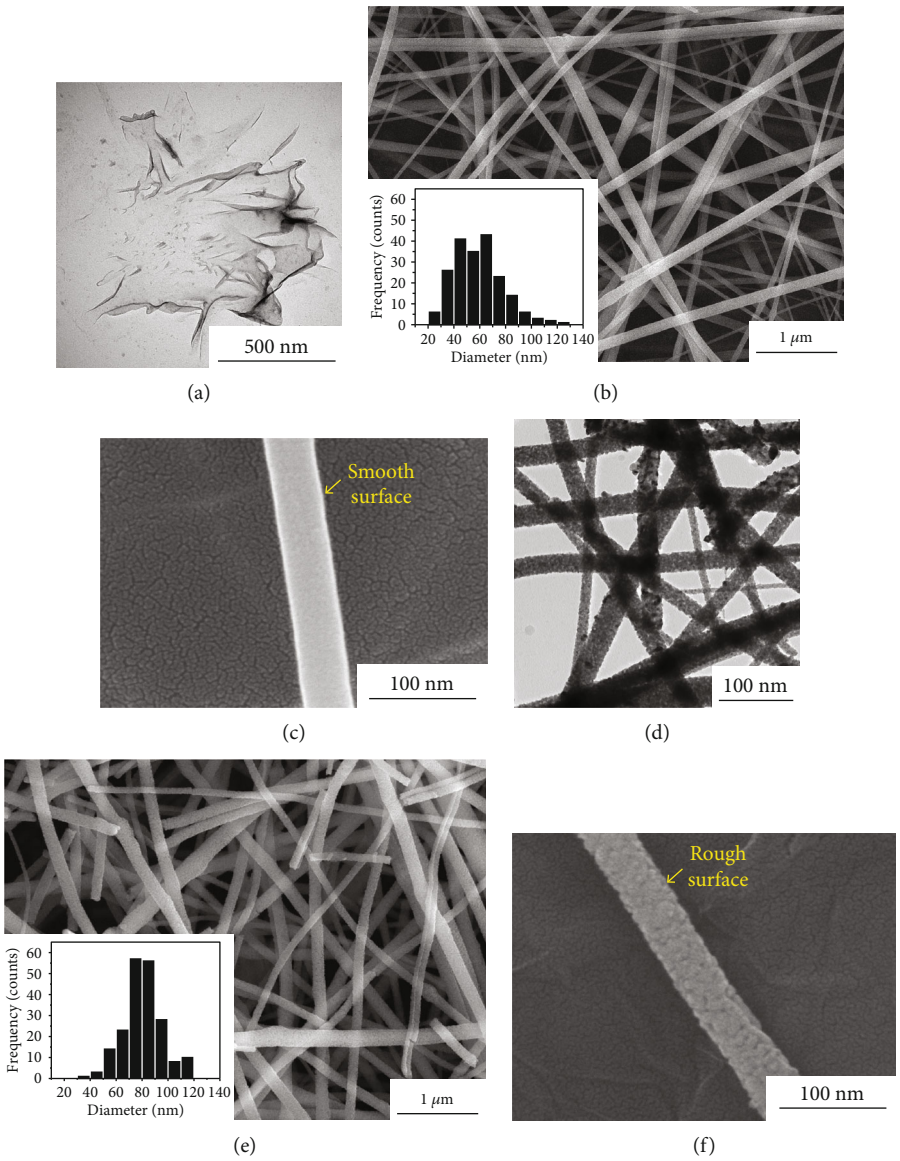

Figure 4: (a) TEM image of GO sheet. SEM images of (b) pristine TiO_2 nanofiber bundle and (c) pristine TiO_2 nanofiber individual with high magnification. (d) TEM image of rGO-wrapped TiO_2 nanofibers. SEM images of (e) rGO-wrapped TiO_2 nanofiber bundle and (f) rGO-wrapped TiO_2 nanofiber individual with high magnification.

Raman spectrum of rGO-wrapped TiO_2 nanofibers refers to the anatase phase but two small peaks at 446 cm^{-1} and 610 cm^{-1}, corresponding to the $B_{1g}(R)$ and $E_g(2)(R)$ modes, respectively. This shows the presence of rutile phase in the rGO-wrapped TiO_2 nanofibers, consistent with the XRD results. In addition, the sp^3 vibration mode of carbon defect peak (D-peak) and sp^2 vibration mode of carbon nature peak (G-peak) can be also observed. However, the D-peak and G-peak were shifted from 1349 to 1350 cm^{-1} and 1608 to 1610 cm^{-1} after the rGO sheets were wrapped around TiO_2 nanofibers. This may be due to the presence of the carbon atoms with rGO defects. Moreover, the I_D/I_G ratio was considered to measure the structural disorder of samples. It can be seen that the I_D/I_G ratio increases from 1.10 to 1.25 because of the increase of sp^3 to sp^2 carbon bonds during the hydrothermal process. The references of Raman spectra for the pure rGO sheets and pristine TiO_2 nanofibers are also displayed in Figures 7(b) and 7(c), respectively.

The UV-Vis spectra of the Kubelka-Munk transformed reflectance are demonstrated in Figure 8. The Tauc plots are displayed to calculate the band gap of pristine TiO_2 and rGO-wrapped TiO_2 nanofibers, according to the following:

$$(\alpha \mathrm{hv})^2 = B_i\left(\mathrm{hv} - E_g\right), \tag{3}$$

where α represents the absorption coefficient, B_i refers to the absorption constant, E_g is the band gap, and hv is the photon energy. The E_g was obtained by the point value of fitted line and x axis from the curve of $(\alpha \mathrm{hv})^2$ and hv energy. The band gap of pristine TiO_2 and rGO-wrapped TiO_2 nanofibers is

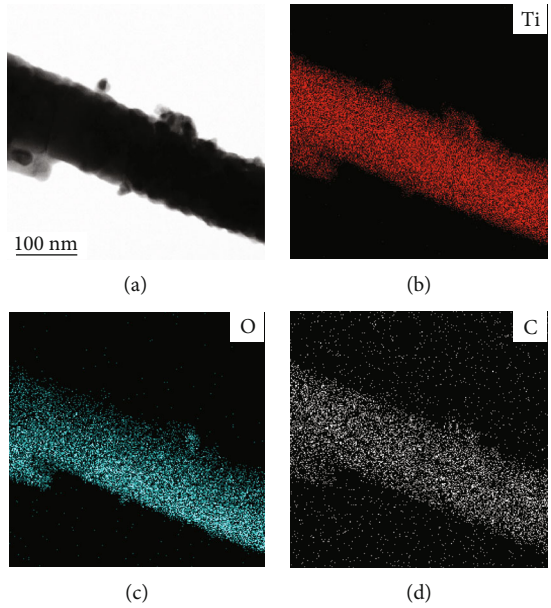

Figure 5: (a) TEM image of rGO-wrapped TiO_2 nanofiber and its elemental map of (b) titanium, (c) oxygen, and (d) carbon.

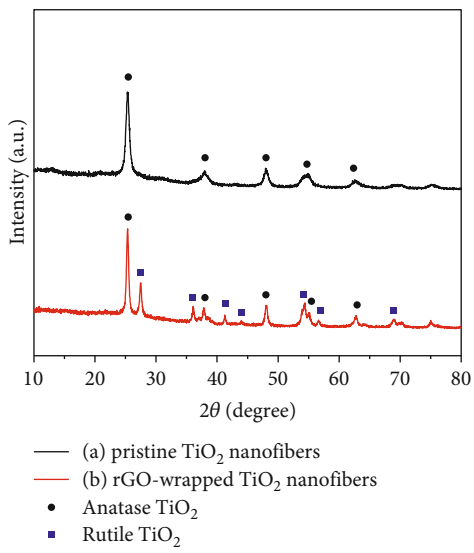

Figure 6: XRD patterns of (a) pristine TiO_2 nanofibers and (b) rGO-wrapped TiO_2 nanofibers.

found to be 3.20 eV (Figure 8(a)) and 2.95 eV (Figure 8(b)), respectively. The decrease of E_g for the rGO-wrapped TiO_2 nanofibers may be due to the shift of the Fermi level by adding the rGO sheets [48]. It may refer to the enhancement of migration for free electrons and repression of electron-hole recombination after the p-n heterojunctions are formed.

3.2. Gas-Sensing Properties. The gas-sensing properties of pristine TiO_2 nanofibers, pure rGO sheets, and rGO-wrapped TiO_2 nanofibers were evaluated by using the gas-measurement system. The changes in resistance of gas sensors were conducted to identify the performances of the sensors. Figure 9 shows the resistance changes of pristine TiO_2

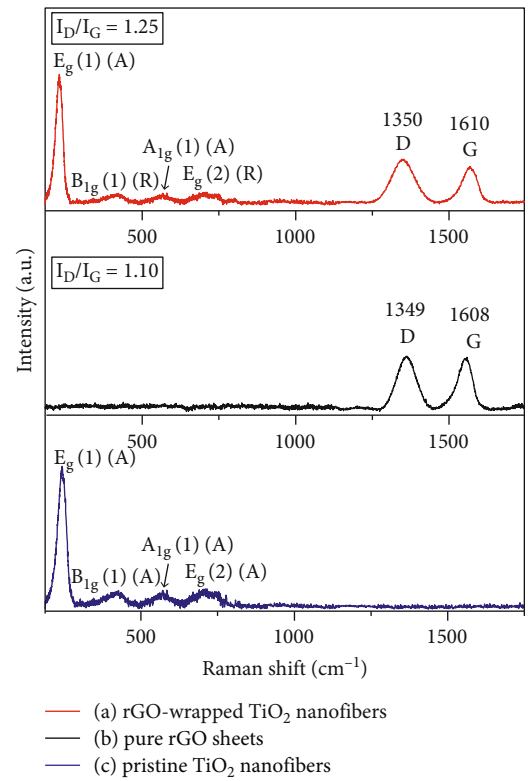

Figure 7: Raman spectra of the synthesized (a) rGO-wrapped TiO_2 nanofibers, (b) pure rGO sheets, and (c) TiO_2 nanofibers.

nanofiber gas sensor exposed to H_2S, C_2H_2, H_2, CH_4, and CO_2 with a concentration of 10, 20, 50, 70, and 100 ppm at room temperature. It can be seen that the baseline resistance of pristine TiO_2 nanofiber gas sensor falls within the order of high resistance (MΩ). Moreover, the sensor resistances do not change obviously under all gases. Therefore, the pristine TiO_2 nanofiber gas sensor does not response or low response

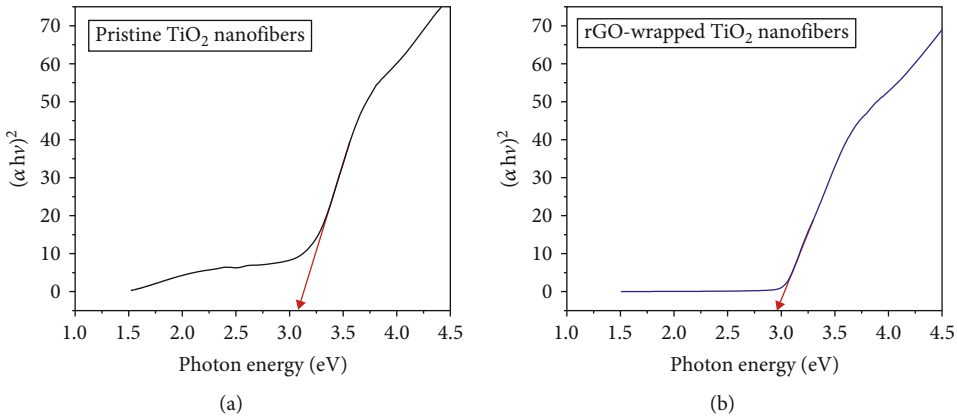

FIGURE 8: Variation of $(\alpha h\nu)^2$ vs. hν of (a) pristine TiO_2 nanofibers and (b) rGO-wrapped TiO_2 nanofibers.

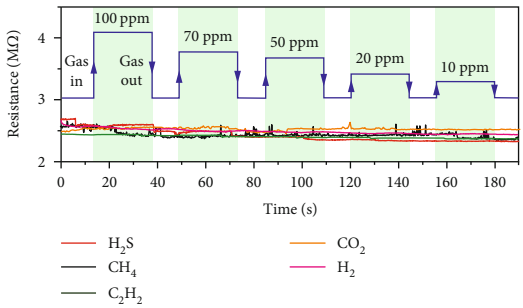

FIGURE 9: Resistance changes of pristine TiO_2 nanofiber gas sensor exposed to various gases with different concentrations at room temperature.

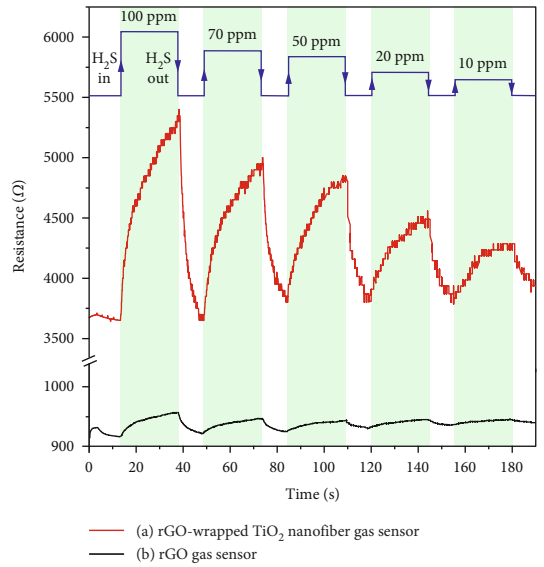

FIGURE 10: Resistance changes of (a) rGO-wrapped TiO_2 nanofiber and (b) rGO gas sensors exposed to H_2S with various concentrations at room temperature.

to all gases at room temperature. These results are consistent with the previous publications [41, 49, 50].

Since the response of pristine TiO_2 nanofiber gas sensor for H_2S sensing is very low at room temperature, only the results of rGO and rGO-wrapped TiO_2 nanofiber gas sensors will be more reported. The changes in resistance of rGO-wrapped TiO_2 nanofiber and rGO gas sensors upon exposure to H_2S with different concentrations from 10 to 100 ppm at room temperature are shown in Figures 10(a) and 10(b), respectively. It can be seen that the rGO-wrapped TiO_2 nanofiber gas sensor shows a high response to H_2S, while the response of rGO gas sensor is very low. In addition, both gas sensors exhibit increments of resistance upon exposure to H_2S before recovering to their baseline lines in dry air. This represents the p-type semiconductor behaviour to a reducing gas. The calculation of gas response is defined by

$$S(\%) = \frac{R_g - R_a}{R_a} \times 100, \quad (4)$$

where R_g and R_a are the resistances of the gas sensor under target gas and dry air, respectively. The calculated values of gas response for the rGO gas sensor exposed to H_2S in the concentrations of 10, 20, 50, 70, and 100 ppm are found to be 0.2, 0.5, 1.61, 2.2, and 2.7%, respectively. In the same concentrations, the values of gas response for the rGO-wrapped TiO_2 nanofiber gas sensors are further found to be 13.3, 16.7, 26.7, 32.1, and 44.6%, respectively. The results affirm the advantage of heterojunction state for rGO-wrapped TiO_2 nanofiber gas sensor in the better H_2S response than pure semiconducting state of rGO gas sensor.

The sensitivity was defined by the slope of linear graph in the relation of gas response versus gas concentration [51–53]. Figure 11(a) shows linear graphs of gas response as a function of H_2S concentration for the rGO-wrapped TiO_2 nanofiber and rGO gas sensors. It can be found that the calculated values of slopes for rGO-wrapped TiO_2 nanofiber and rGO gas sensors are 0.341 and 0.029 ppm^{-1}, respectively. The coefficients of determination (R^2) for rGO-wrapped TiO_2 nanofiber and rGO gas sensors fitted and calculated by OriginLab software are also found to be 0.994 and 0.973, respectively. Therefore, the wrapping of rGO sheets around TiO_2 nanofibers leads to a better sensitivity of the H_2S gas sensor at room temperature. The response time

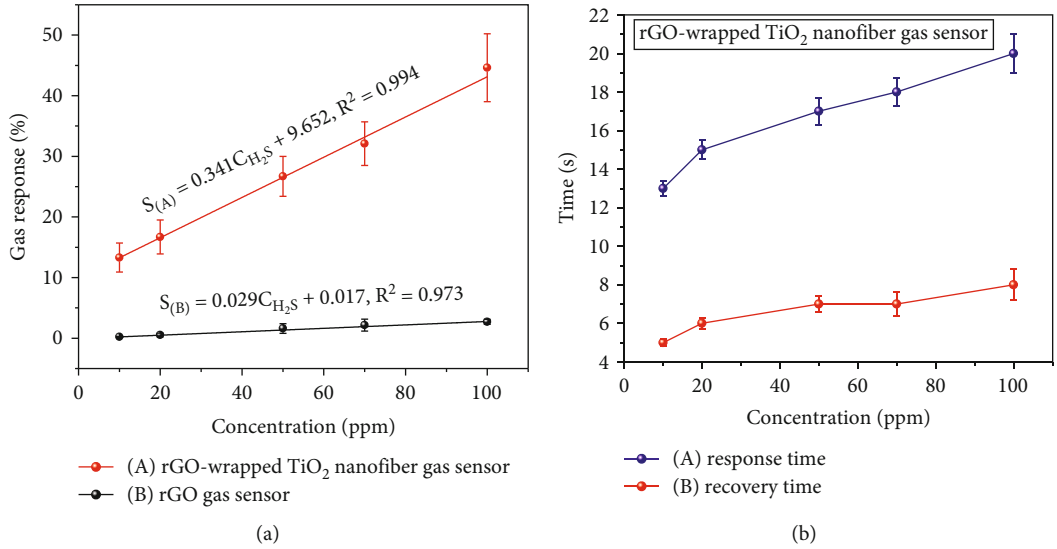

Figure 11: (a) Gas responses of rGO-wrapped TiO_2 nanofiber and rGO gas sensors and (b) response/recovery times of rGO-wrapped TiO_2 nanofiber gas sensor as a function of H_2S concentration at room temperature.

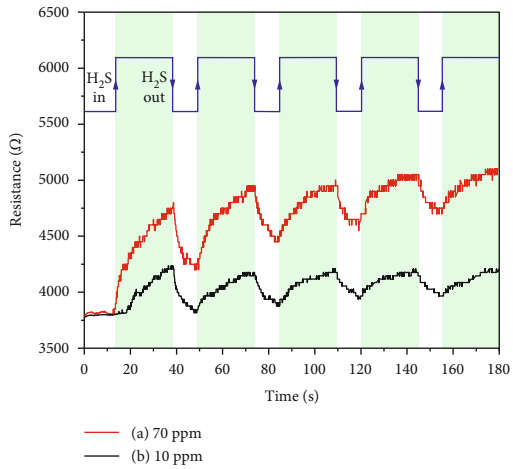

Figure 12: Resistance changes of rGO-wrapped TiO_2 nanofiber gas sensor exposed to H_2S with concentrations of (a) 70 ppm and (b) 10 ppm at room temperature.

was defined as the time to reach 90% of the change for the sensor resistance after exposure to a target gas [51–53]. For the recovery time, it was further defined as the time for recovering the sensor resistance to its baseline after the target gas was suddenly cut off [51–53]. The trend lines of response and recovery times for rGO-wrapped TiO_2 nanofiber gas sensor exposed to H_2S with various concentrations at room temperature are shown in Figure 11(b). It is seen that the recovery time of sensor is faster than the response time. Moreover, the response time increases from 13.0 s to 20.0 s when the concentration of H_2S increases from 10 to 100 sccm, whereas the recovery time of sensor also increases from 5.0 to 8.0 s. Therefore, the response/recovery times of sensor increase with increasing H_2S concentrations.

The changes in resistance of rGO-wrapped TiO_2 nanofiber sensors upon exposure to H_2S with concentrations of 70 and 10 ppm are displayed in Figures 12(a) and 12(b), respectively. It can be seen that the resistance of sensor exposed to 70 ppm H_2S could not return back to its baseline resistance. This is due to the fact that the H_2S molecules with high concentration cannot fully purge off from the sensor surface by the air under ambient condition. This cause leads to the drift of baseline resistance for the gas sensor after testing in every cycle. For the rGO-wrapped TiO_2 nanofiber sensor under 10 ppm H_2S, it can be observed that the resistance of sensor immediately decreases and nearly recovers to its baseline resistance over 4 cycles. This is due to the almost complete desorption of H_2S molecules after the purging process.

As can be found from the preliminary results, the thickness of rGO wrapped around the TiO_2 nanofibers is dependent on the GO content. The SEM image of rGO-wrapped TiO_2 nanofiber prepared by 100 mg of GO powder is shown in Figure 13(a). It is clearly seen that there are some thick rGO sheets around the TiO_2 nanofiber. The nearby rGO sheets could be merged and formed into larger sheets under a condition of high GO content. Moreover, we have already investigated the effect of GO content on the H_2S response of rGO-wrapped TiO_2 nanofiber gas sensor at room temperature. It should be noted that the GO powder was dissolved in 20 ml DMSO and 20 ml DI water followed by the addition of 70 mg TiO_2 nanofibers before the rGO-wrapped TiO_2 nanofibers were formed by hydrothermal process. As shown in Figure 13(b), the values of H_2S response for the sensor under different GO contents of 20, 50, 75, and 100 mg are found to be 22.4, 44.6, 10.2, and 7.9%, respectively. These results show that the optimal content of GO powder for wrapping the rGO around the TiO_2 nanofiber to obtain an effective room-temperature H_2S gas sensor is 50 mg. In the case of rGO-wrapped TiO_2 nanofiber gas sensor with high content of GO (75 and 100 mg), the response of sensor is low because the number of charge carriers in rGO-wrapped TiO_2 nanofibers is much higher than the charge transfer. This explanation is consistent with a previous work of another group. They have reported about the low

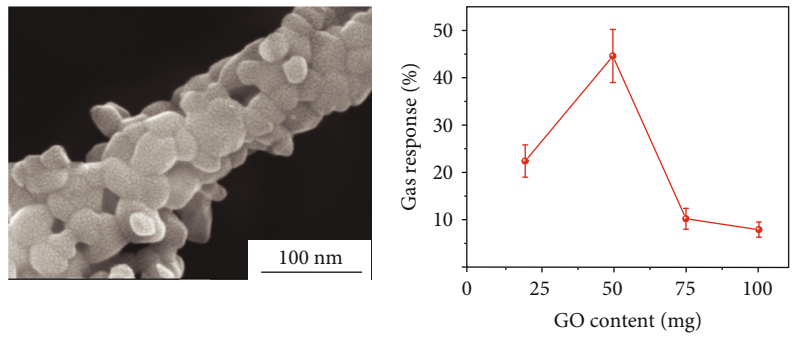

FIGURE 13: (a) SEM image of rGO-wrapped TiO_2 nanofiber prepared by 100 mg of GO powder. (b) Gas responses of rGO-wrapped TiO_2 nanofiber gas sensor as a function of prepared GO content.

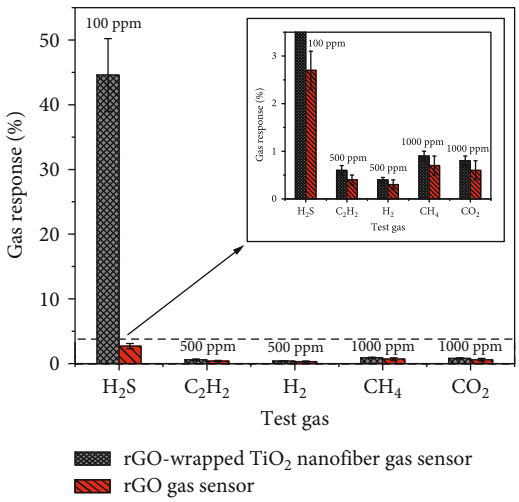

FIGURE 14: Selectivity histogram of rGO-wrapped TiO_2 nanofiber and rGO gas sensors exposed to various gases with different concentrations at room temperature.

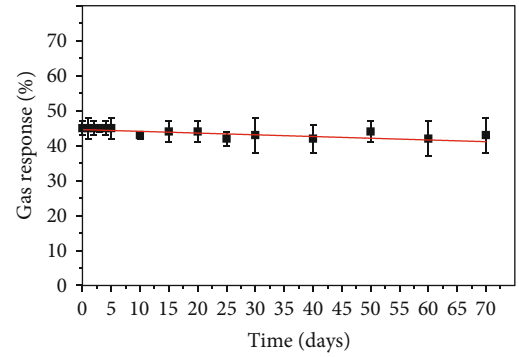

FIGURE 15: Long-term stability measurement of rGO-wrapped TiO_2 nanofiber gas sensor in a period of 70 days upon repetitive exposure to 100 ppm H_2S at room temperature.

response of three-dimensional graphene-carbon nanotube nanostructures to toluene under the condition of high carbon content [54].

The generated p-n heterojunctions of nanocomposite materials have been affirmed by baseline resistance of gas sensor [54, 55]. For the n-type semiconducting TiO_2 gas sensor, it is well known that electrons are the most common type of charge carrier. The decrease in baseline resistance of n-type metal oxide and p-type carbon materials can be attributed to the increased electron concentration due to the formation of p-n heterojunctions. In this work, the baseline resistance of pristine TiO_2 nanofiber gas sensor falls within ~2.5 MΩ while the baseline resistance of rGO-wrapped TiO_2 nanofiber is found to be ~3.7 kΩ. This could be affirmed to the formation of p-n heterojunctions between TiO_2 nanofibers and rGO sheets.

Figure 14 shows the selectivity histogram of rGO-wrapped TiO_2 nanofiber and rGO gas sensors toward different gases, including 100 ppm H_2S, 500 ppm C_2H_2, 500 ppm H_2, 1000 ppm CH_4, and 1000 ppm CO_2 at room temperature. It is seen that the rGO-wrapped TiO_2 nanofiber gas sensor exhibits a high response to H_2S and low responses to C_2H_2, H_2, CH_4, and CO_2, while the rGO gas sensor shows the low responses to all gases. It is well known that the gas response of sensor increases with increasing gas concentration. Although the concentrations of the C_2H_2, H_2, CH_4, and CO_2 are added more to over 500 ppm, the very low responses to the gases for the both sensors are still observed. These results confirm the good selectivity of rGO-wrapped TiO_2 nanofiber gas sensor to H_2S at room temperature.

The H_2S-sensing measurement of rGO-wrapped TiO_2 nanofiber gas sensor was further repeated for 70 days, as shown in Figure 15. The long-term stability with only ~5% of reduction from its initial response under room-temperature storage indicates that the gas responses are almost stable under ambient conditions. Moreover, the H_2S-sensing performance of the room-temperature rGO-wrapped TiO_2 nanofiber gas sensor in this work is superior to previous works, as listed in Table 1. Although there have been some works revealing the sensor performance in higher H_2S response, the high operation temperature of them is still an obstacle [41, 56].

The H_2S-sensing mechanisms of rGO-wrapped TiO_2 nanofiber gas sensor have been discussed based on two possible mechanisms such as the formation of p-n heterojunctions and the direct charge-transfer process. The free electrons in rGO regions will transfer to TiO_2 nanofibers when the heterojunctions are formed. This cause results in a depletion of electrons on the rGO surfaces [37]. It leads

Table 1: Comparison of H_2S gas sensors from previous works and this work.

Materials	Operating temperature (°C)	Response (%)	Response definition	H_2S concentration (ppm)	Ref.
Fe_2O_3 decorated CuO nanorods	150	4.0	R_g/R_a	5	[8]
Ag-doped Fe_2O_3 hollow nanofibers	RT	19.4	R_a/R_g	100	[11]
Cu-doped ZnO/rGO	RT	1.3	$(R_g - R_a)/R_a \times 100$	250	[12]
SnO_2-Fe_2O_3 nanoparticles	55	14.9	$(I_g - I_a)/I_a$	2.5	[16]
Ag-doped TiO_2	350	240	$(R_g - R_a)/R_a \times 100$	10	[41]
2D MoO_3 nanoflakes	300	75	$(R_g - R_a)/R_a \times 100$	10	[56]
rGO-wrapped TiO_2 nanofibers	RT	44.6	$(R_g - R_a)/R_a \times 100$	100	This work

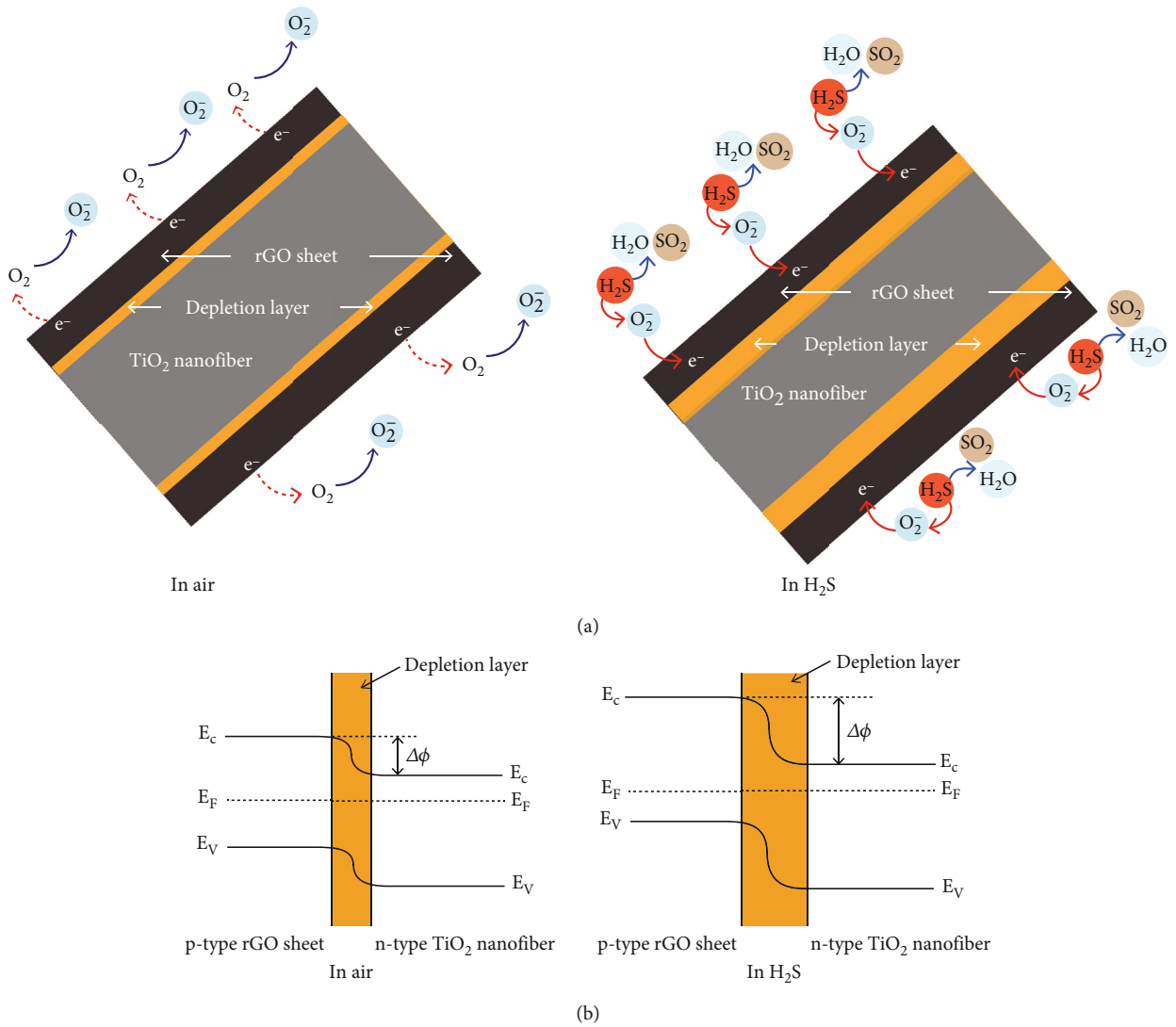

Figure 16: (a) Schematic illustration of H_2S-sensing mechanism and (b) p-n heterojunction of rGO-wrapped TiO_2 nanofiber gas sensor.

to the bending of energy band in n-type semiconducting TiO_2 nanofiber, causing an increase of baseline resistance from ~0.93 kΩ to ~3.54 kΩ after wrapping the rGO on the TiO_2 nanostructures (see Figure 10). In air, the chemisorbed oxygen groups will trap free electrons from the conduction band of TiO_2 and the Fermi level of rGO, according to the

reaction: O_2 (ads) + $e^- \longrightarrow O_2^-$ (ads) [37]. It should be noted that H_2S represents a reducing gas property. When rGO-wrapped TiO_2 nanofiber gas sensor is exposed to H_2S, the gas molecules will react with adsorbed oxygen groups. The free electrons trapped by O_2^- groups will return back to conduction band of rGO-wrapped TiO_2 nanofibers, resulting in the increase of resistance of p-type semiconducting gas sensor. The reaction can be labeled as follows: $2H_2S$ (g) + $3O_2^-$ (ads) $\longrightarrow 2H_2O$ (g) + $2SO_2$ (g) + $3e^-$ [28, 57]. The schematic illustration of the proposed H_2S-sensing mechanism is illustrated in Figure 16(a). The increase of resistance for the gas sensor upon exposure to H_2S can be explained by the increase of the height for the potential barrier at p-n heterojunction, according to the following:

$$R = R_o e^{\Delta \varnothing q/kT}. \quad (5)$$

where R is the sensor resistance, R_o is a constant, q is the charge of electron, $\Delta\phi$ is the height of potential barrier at p-n heterojunction, k is Boltzmann's constant, and T is the sensing-layer temperature [37, 54]. The p-n heterojunction of rGO-wrapped TiO_2 nanofiber gas sensor is illustrated in Figure 16(b). The nonrecovery of resistance for the sensor under high H_2S concentration was presented after the stream of H_2S gas was cut off. This is due to the highly strong bonding between H_2S molecules and oxygen containing groups on rGO-wrapped TiO_2 nanofiber surface. This may lead to a creation of baseline drift for the resistance of the rGO-wrapped TiO_2 nanofibers at the higher concentration of H_2S (70 ppm).

For the second possible mechanism, the rGO-wrapped TiO_2 nanofiber gas sensor is exposed to lower concentration of H_2S (10 ppm). It has been discussed based on the direct charge-transfer process between H_2S molecules and rGO-wrapped TiO_2 nanofiber surfaces by physisorption. The Van der Waals interaction has been considered as a dominant action in the presentation of this possible mechanism. The increments in the active areas and π-π interactions can be improved by the wrapping of rGO sheets around TiO_2 nanofibers. When the H_2S molecules are adsorbed onto active areas of rGO-wrapped TiO_2 nanofiber, the holes of rGO-wrapped TiO_2 nanofiber will react to free electrons from H_2S molecules. Then, the resistance of the p-type semiconducting rGO-wrapped TiO_2 nanofiber gas sensor increases. Moreover, the H_2S molecules can be easily purged under dry air at room temperature due to the weak interactions of physisorption. This cause may lead to the near complete recovery of the baseline resistance for the gas sensor under lower concentration of H_2S (10 ppm).

4. Conclusions

The rGO-wrapped TiO_2 nanofibers were successfully synthesized by the combination of electrospinning and hydrothermal methods. The confirmation of existence for rGO sheets on the surface of TiO_2 nanofibers was characterized by SEM, TEM, XRD, and Raman spectroscopy. The UV-Vis spectra were employed to investigate the band gaps of nanofibers before and after wrapping the rGO sheets on the surface of TiO_2 nanofibers. The nanofibers were evaluated for H_2S adsorption at room temperature. As the results, the rGO-wrapped TiO_2 nanofiber gas sensor presented a p-type semiconducting behaviour and good response upon exposure to H_2S at room temperature. The hydrothermal wrapping of rGO sheets around the TiO_2 nanofibers with an optimal GO content of 50 mg led to the optimal enhancement of H_2S response at room temperature. Moreover, the rGO-wrapped TiO_2 nanofiber gas sensor exhibited a good selectivity and long-term stability toward H_2S as well. The H_2S-sensing mechanism of rGO-wrapped TiO_2 nanofibers gas sensor was proposed based on the formation of p-n heterojunctions of p-type rGO sheets and n-type TiO_2 nanofibers. Finally, the direct charge-transfer process between H_2S molecules and rGO-wrapped TiO_2 nanofiber surfaces by physisorption was mentioned as a second possible H_2S-sensing mechanism. All the results proved that the rGO-wrapped TiO_2 nanofibers can be considered as a good selection for applications in H_2S adsorption at room temperature.

Data Availability

The data used to support the findings of this study are available from the corresponding author upon request.

Conflicts of Interest

The authors declare that there is no conflict of interests regarding the publication of this paper.

Acknowledgments

The authors would like to thank for gas measurements and facilities provided by Dr. Anurat Wisitsoraat from Carbon-based Devices and Nanoelectronics Laboratory, National Electronics and Computer Technology Center, Thailand. This work was financially supported by the Research and Development Institute, Rajamangala University of Technology Krungthep, Thailand (Grant No. ST-1045).

References

[1] B. Doujaiji and J. A. Al-Tawfiq, "Hydrogen sulfide exposure in an adult male," *Annals of Saudi Medicine*, vol. 30, no. 1, pp. 76–80, 2010.

[2] A. Sampaolo, C. Yu, T. Wei et al., "H_2S quartz-enhanced photoacoustic spectroscopy sensor employing a liquid-nitrogen-cooled THz quantum cascade laser operating in pulsed mode," *Photoacoustics*, vol. 21, article 100219, 2021.

[3] Š. Brglez, "Risk assessment of toxic hydrogen sulfide concentrations on swine farms," *Journal of Cleaner Production*, vol. 312, article 127746, 2021.

[4] G. F. Fine, L. M. Cavanagh, A. Afonja, and R. Binions, "Metal oxide semi-conductor gas sensors in environmental monitoring," *Sensors*, vol. 10, no. 6, pp. 5469–5502, 2010.

[5] A. I. Ayesh, "Metal/metal-oxide nanoclusters for gas sensor applications," *Journal of Nanomaterials*, vol. 2016, Article ID 2359019, 17 pages, 2016.

[6] A. Dey, "Semiconductor metal oxide gas sensors: a review," *Materials Science and Engineering: B*, vol. 229, pp. 206–217, 2018.

[7] V. Kumar, S. Sen, K. P. Muthe, N. K. Gaur, S. K. Gupta, and J. V. Yakhmi, "Copper doped SnO_2 nanowires as highly sensitive H_2S gas sensor," *Sensors and Actuators B*, vol. 138, no. 2, pp. 587–590, 2009.

[8] S. Park, Z. Cai, J. Lee, J. I. Yoon, and S.-P. Chang, "Fabrication of a low-concentration H_2S gas sensor using CuO nanorods decorated with Fe_2O_3 nanoparticles," *Materials Letters*, vol. 181, pp. 231–235, 2016.

[9] Y. XueJun, H. TianSheng, Y. Zhou, and H. ShuangPing, "Room temperature H_2S micro-sensors with anti-humidity properties fabricated from NiO-In_2O_3 composite nanofibers," *Chinese Science Bulletin*, vol. 58, no. 7, pp. 821–826, 2013.

[10] G. Jiang, J. Keller, and P. L. Bond, "Determining the long-term effects of H_2S concentration, relative humidity and air temperature on concrete sewer corrosion," *Water Resources Research*, vol. 65, pp. 157–169, 2014.

[11] C. Yang, Y. Yang, C. Zhang et al., "High selectivity of Ag-doped Fe_2O_3 hollow nanofibers in H_2S detection at room operating temperature," *Sensors and Actuators B*, vol. 341, article 129919, 2021.

[12] P. S. Shewale and K.-S. Yun, "Synthesis and characterization of Cu-doped ZnO/RGO nanocomposites for room- temperature H_2S gas sensor," *Journal of Alloys and Compounds*, vol. 837, article 155527, 2020.

[13] P.-G. Su and Y.-T. Peng, "Fabrication of a room-temperature H_2S gas sensor based on PPy/WO_3 nanocomposite films by *in-situ* photopolymerization," *Sensors and Actuators B*, vol. 193, pp. 637–643, 2014.

[14] S. Kanaparthi and S. G. Singh, "Drift independent discrimination of H_2S from other interfering gases with a metal oxide gas sensor using extracted adsorption- desorption noise," *Sensors and Actuators B*, vol. 344, article 130146, 2021.

[15] A. Mirzaei, S. S. Kim, and H. W. Kim, "Resistance-based H_2S gas sensors using metal oxide nanostructures: a review of recent advances," *Journal of Hazardous Materials*, vol. 357, pp. 314–331, 2018.

[16] B. Salah and A. I. Ayesh, "Fabrication of H_2S sensitive gas sensors formed of SnO_2-Fe_2O_3 composite nanoparticles," *Materials Chemistry and Physics*, vol. 266, article 124597, 2021.

[17] L. Ruiz-Rodríguez, A. de Arriba, A. Vidal-Moya, T. Blasco, E. Rodríguez-Castellón, and J. M. L. Nieto, "The role of promoters on the catalytic performance of $M_xV_2O_5$ bronzes for the selective partial oxidation of H_2S," *Applied Catalysis A, General*, vol. 647, article 118900, 2022.

[18] H. Cao, B. Li, J. Zhang, F. Lian, X. Kong, and M. Qu, "Synthesis and superior anode performance of TiO_2@reduced graphene oxide nanocomposites for lithium ion batteries," *Journal of Materials Chemistry*, vol. 22, no. 19, p. 9759, 2012.

[19] L. Thirugunanam, S. Kaveri, V. Etacheri, S. Ramaprabhu, M. Dutta, and V. G. Pol, "Electrospun nanoporous TiO_2 nanofibers wrapped with reduced graphene oxide for enhanced and rapid lithium-ion storage," *Materials Characterization*, vol. 131, pp. 64–71, 2017.

[20] A. A. Nada, M. F. Bekheet, R. Viter, P. Miele, S. Roualdes, and M. Bechelany, "BN/$Gd_xTi_{(1-x)}O_{(4-x)/2}$ nanofibers for enhanced photocatalytic hydrogen production under visible light," *Applied Catalysis B: Environmental*, vol. 251, pp. 76–86, 2019.

[21] E. A. Nada, H. H. El-Maghrabi, P. Raynaud et al., "Enhanced photocatalytic activity of WS_2/TiO_2 nanofibers for degradation of phenol under visible light irradiation," *Inorganics*, vol. 10, no. 4, p. 54, 2022.

[22] M. Ghorbanloo, A. A. Nada, H. H. El-Maghrabi et al., "BN/Cs_2CO_3/TiO_2 composite nanofibers to improve hydrogen generation," *Journal of Alloys and Compounds*, vol. 945, article 169218, 2023.

[23] X. Tian, X. Cui, T. Lai et al., "Gas sensors based on TiO_2 nanostructured materials for the detection of hazardous gases: a review," *Nano Materials Science*, vol. 3, no. 4, pp. 390–403, 2021.

[24] N. Chen, Y. Li, D. Deng et al., "Acetone sensing performances based on nanoporous TiO_2 synthesized by a facile hydrothermal method," *Sensors and Actuators B*, vol. 238, pp. 491–500, 2017.

[25] S. Cao, N. Sui, P. Zhang, T. Zhou, J. Tu, and T. Zhang, "TiO_2 nanostructures with different crystal phases for sensitive acetone gas sensors," *Journal of Colloid and Interface Science*, vol. 607, Part 1, pp. 357–366, 2022.

[26] S. H. Salman, A. A. Shihab, and A.-H. K. Elttayef, "Design and construction of nanostructure TiO_2 thin film gas sensor prepared by r.f magnetron sputtering technique," *Energy Procedia*, vol. 157, pp. 283–289, 2019.

[27] M. Wang, Y. Zhu, D. Meng, K. Wang, and C. Wang, "A novel room temperature ethanol gas sensor based on 3D hierarchical flower- like TiO_2 microstructures," *Materials Letters*, vol. 277, article 128372, 2020.

[28] Nagmani, D. Pravarthana, A. Tyagi, T. C. Jagadale, W. Prellier, and D. K. Aswal, "Highly sensitive and selective H_2S gas sensor based on TiO_2 thin films," *Applied Surface Science*, vol. 549, article 149281, 2021.

[29] Y. M. Sabri, A. E. Kandjani, S. S. A. A. H. Rashid, C. J. Harrison, S. J. Ippolito, and S. K. Bhargava, "Soot template TiO_2 fractals as a photoactive gas sensor for acetone detection," *Sensors and Actuators B*, vol. 275, pp. 215–222, 2018.

[30] Á. Peña, D. Matatagui, F. Ricciardella et al., "Optimization of multilayer graphene-based gas sensors by ultraviolet photoactivation," *Applied Surface Science*, vol. 610, article 155393, 2023.

[31] S. Yeo, C. Y. Lee, D.-S. Kim et al., "Sensing response enhancement of graphene gas sensors by ion beam bombardment," *Thin Solid Films*, vol. 677, pp. 73–76, 2019.

[32] S. Huang, L. A. Panes-Ruiz, A. Croy et al., "Highly sensitive room temperature ammonia gas sensor using pristine graphene: the role of biocompatible stabilizer," *Carbon*, vol. 173, pp. 262–270, 2021.

[33] G. Imamura, K. Minami, K. Shiba et al., "Graphene oxide as a sensing material for gas detection based on nanomechanical sensors in the static mode," *Chemosensors*, vol. 8, no. 3, p. 82, 2020.

[34] A. Lipatov, A. Varezhnikov, P. Wilson, V. Sysoev, A. Kolmakov, and A. Sinitskii, "Highly selective gas sensor arrays based on thermally reduced graphene oxide," *Nanoscale*, vol. 5, no. 12, pp. 5426–5434, 2013.

[35] K. Lee, Y. K. Yoo, M.-S. Chae et al., "Highly selective reduced graphene oxide (rGO) sensor based on a peptide aptamer receptor for detecting explosives," *Scientific Reports*, vol. 9, no. 1, article 10297, 2019.

[36] M. Yang, Y. Wang, L. Dong et al., "Gas sensors based on chemically reduced holey graphene oxide thin films," *Nanoscale Research Letters*, vol. 14, no. 1, p. 218, 2019.

[37] Y. Seekaew, W. Pon-On, and C. Wongchoosuk, "Ultrahigh selective room-temperature ammonia gas sensor based on tin –titanium dioxide/reduced graphene/carbon nanotube nanocomposites by the solvothermal method," *ACS Omega*, vol. 4, no. 16, pp. 16916–16924, 2019.

[38] J.-H. Lee, A. Katoch, S.-W. Choi, J.-H. Kim, H. W. Kim, and S. S. Kim, "Extraordinary improvement of gas-sensing performances in SnO_2 nanofibers due to creation of local p-n heterojunctions by loading reduced graphene oxide nanosheets," *ACS Applied Materials & Interfaces*, vol. 7, no. 5, pp. 3101–3109, 2015.

[39] S. M. Majhi, A. Mirzaei, H. W. Kim, and S. S. Kim, "Reduced graphene oxide (rGO)-loaded metal-oxide nanofiber gas sensors: an overview," *Sensors*, vol. 21, no. 4, p. 1352, 2021.

[40] D. Wang, M. Tang, and J. Sun, "Direct fabrication of reduced graphene oxide@SnO_2 hollow nanofibers by single-capillary electrospinning as fast NO_2 gas sensor," *Journal of Nanomaterials*, vol. 2019, Article ID 1929540, 7 pages, 2019.

[41] S. Ma, J. Jia, Y. Tian et al., "Improved H_2S sensing properties of Ag/TiO_2 nanofibers," *Ceramics International*, vol. 42, no. 1, pp. 2041–2044, 2016.

[42] Y. J. Yun, W. G. Hong, N.-J. Choi et al., "A 3D scaffold for ultra-sensitive reduced graphene oxide gas sensors," *Nanoscale*, vol. 6, no. 12, pp. 6511–6514, 2014.

[43] A. A. Nada, B. O. Orimolade, H. H. El-Maghrabi et al., "Photoelectrocatalysis of paracetamol on Pd-ZnO/ N-doped carbon nanofibers electrode," *Applied Materials Today*, vol. 24, article 101129, 2021.

[44] D. Xu, L. Li, R. He, L. Qi, L. Zhang, and B. Cheng, "Noble metal-free RGO/TiO_2 composite nanofiber with enhanced photocatalytic H_2-production performance," *Applied Surface Science*, vol. 434, pp. 620–625, 2018.

[45] B. Anitha and M. A. Khadar, "Anatase-rutile phase transformation and photocatalysis in peroxide gel route prepared TiO_2 nanocrystals: Role of defect states," *Solid State Sciences*, vol. 108, article 106392, 2020.

[46] G. T. S. How, A. Pandikumar, H. N. Ming, and L. H. Ngee, "Highly exposed {001} facets of titanium dioxide modified with reduced graphene oxide for dopamine sensing," *Scientific Reports*, vol. 4, no. 1, p. 5044, 2014.

[47] C. Kuchi, B. Naresh, and P. S. Reddy, "In situ TiO_2-rGO nanocomposite for low concentration NO gas sensor," *ECS Journal of Solid State Science and Technology*, vol. 10, no. 3, article 037008, 2021.

[48] P.-G. Su and Y.-L. Zheng, "Room-temperature ppb-level SO2gas sensors based on $_{RGO/WO3and}$ MWCNTs/WO3nanocomposites," *Analytical Methods*, vol. 13, no. 6, pp. 782–788, 2021.

[49] X. Tong, W. Shen, X. Chen, and J.-P. Corriou, "A fast response and recovery H_2S gas sensor based on free-standing TiO_2 nanotube array films prepared by one-step anodization method," *Ceramics International*, vol. 43, no. 16, pp. 14200–14209, 2017.

[50] D. Zhang, C. Jiang, and X. Zhou, "Fabrication of Pd-decorated TiO_2/MoS_2 ternary nanocomposite for enhanced benzene gas sensing performance at room temperature," *Talanta*, vol. 182, pp. 324–332, 2018.

[51] U. Pakdee and A. Thaibunnak, "Growth of MWCNTs on plasma ion-bombarded thin gold films and their enhancements of ammonia-sensing properties using inkjet printing," *Journal of Nanotechnology*, vol. 2019, Article ID 3424915, 11 pages, 2019.

[52] A. Thaibunnak and U. Pakdee, "Pen-based writing of functionalized MWCNT-PEDOT:PSS ink on flexible substrate for application in ammonia gas sensor," *Suranaree Journal of Science and Technology*, vol. 29, article 010119, 2022.

[53] D. Boonthum, C. Oopathump, S. Fuengfung et al., "Screen-printing of functionalized MWCNT-PEDOT:PSS based solutions on bendable substrate for ammonia gas sensing," *Micromachines*, vol. 13, no. 3, p. 462, 2022.

[54] Y. Seekaew, A. Wisitsoraat, D. Phokharatkul, and C. Wongchoosuk, "Room temperature toluene gas sensor based on TiO_2 nanoparticles decorated 3D graphene-carbon nanotube nanostructures," *Sensors and Actuators B*, vol. 279, pp. 69–78, 2019.

[55] Y. Seekaew, A. Wisitsoraat, and C. Wongchoosuk, "ZnO quantum dots decorated carbon nanotubes-based sensors for methanol detection at room temperature," *Diamond & Related Materials*, vol. 132, article 109630, 2023.

[56] J. Bao, Z. Zhang, and Y. Zheng, "H_2S sensor based on two-dimensional MoO_3 nanoflakes: transition between sulfidation and oxidation," *Sensors and Actuators B: Chemical*, vol. 345, article 130408, 2021.

[57] Z. S. Hosseini, A. Iraji zad, and A. Mortezaali, "Room temperature H_2S gas sensor based on rather aligned ZnO nanorods with flower-like structures," *Sensors and Actuators B: Chemical*, vol. 207, pp. 865–871, 2015.